ACS Sustainable Chemistry & Engineering

pubs.acs.org/journal/ascecg

Research Article

# Role of Reactant Alkylation Grade in the Selectivity and Stability of Furan−Alkene Diels−Alder Reactions

Juan Gancedo, Laura Faba, and Salvador Ordóñez*

Cite This: *ACS Sustainable Chem. Eng.* 2022, 10, 3057−3065

Read Online

ACCESS | Metrics & More | Article Recommendations | Supporting Information

**ABSTRACT:** Diels−Alder condensation between different bio-based furanic compounds and light alkenes was performed in a fixed-bed reactor using ZSM-5 zeolite as a catalyst, analyzing the role of the alkylation of both reactants in this gas-phase reaction. The effect of this alkylation on product distribution and catalyst stability was thoroughly studied. These two aspects are the critical drawbacks in the production of aromatics from biomass-derived carbonylic compounds. The use of alkylated furans and alkenes promotes monoaromatic formation and their subsequent alkylation, minimizing the production of secondary condensation byproducts, such as naphthalenes and coke. This fact significantly improves the stability of the aromatic production without affecting the regeneration capacity of the zeolite. The methylfuran−propylene system is proposed as the most promising one for this purpose, increasing the selectivity to benzenes by 22% and the stability by 77%, concerning the results obtained with the methylfuran−ethylene system.

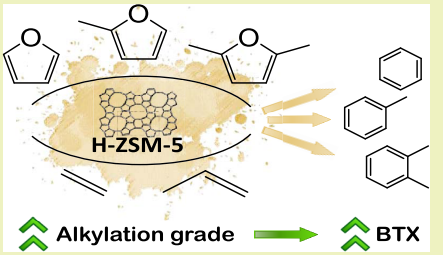


**KEYWORDS:** *biomass pyrolysis, BTX, catalyst deactivation, ZSM-5, coke, renewable aromatics*



## INTRODUCTION

Diels−Alder condensation is one of the most promising routes to obtain aromatics from renewable resources, drawing the attention of researchers as an alternative to petrochemical routes.[1] This reaction is typically catalyzed by acid zeolites and involves a cycloaddition of a conjugated diene (furan) and a dienophile (alkene). The reactants' origin determines the sustainability of the process. In this context, not only furan but also (poly)alkyl furans could be relevant reactants, obtained from biomass by different routes, such as lignocellulose hydrolysis and hydrogenolysis or dehydration.[2−5]

Depending on the furan alkylation grade and the alkene chain length, the direct reaction promotes benzene, toluene, or xylene (BTX) as the main products. However, the complex product distribution with the subsequent low selectivity in the final mixture, including not only BTX but also naphthalenes, indenes, etc., is considered as one of its main drawbacks of this approach.[6] The general mechanism is depicted in Scheme 1. It includes not only the different condensations but also alkylation, dealkylation, and disproportionation reactions. Considering the industrial interest, several researchers have studied this reaction to improve the BTX selectivity, concluding that temperatures in the range of 500−550 °C, the low WHSV, and low partial pressures are the optimum ones to maximize this fraction.[7−9] As for the catalyst, acid ZSM-5 and $\beta$ zeolites are highlighted in the literature,[10,11] both in their protonated form or including metals, such as Ga,[12−14] Zn,[15] MgO,[16] Zr, or Sn.[17,18]

The second main drawback of this process is the presence of catalyst deactivation due to the uncontrolled coke deposition on the catalytic surface.[6] This fact limits the industrial application of this approach, justifying the recent studies focused on studying the reaction conditions that reduce this coking.[19−21] Despite these works, understanding of coke formation chemistry in this reaction system is still limited. As a general conclusion, the zeolite deactivation is produced by a mixture of two types of carbonaceous deposits, oxygenated and graphitic coke, which block the pores and, subsequently, the active sites. Benzofuran, produced by condensation between two furans, is considered the main precursor of the oxygenated coke.[22] Working with an excess of alkenes at temperatures high enough to promote the Diels−Alder step over the self-condensation of furans is identified as good conditions to reduce the deactivation by this route.[23]

These conditions can enhance subsequent oligomerizations and condensations of BTX with furans, yielding naphthalenes, polycyclic aromatic hydrocarbons (PAHs), and finally, graphitic-type coke.[20] This well-ordered coke can also be obtained by the stabilization of the oxygenated one by different Diels−Alder and decarbonylation reactions, significantly reducing the oxygen content and, subsequently, increasing the crystallinity of these deposits. To sum up, the control on the catalytic stability and coke prevention is a difficult aspect of this process.

Received: December 23, 2021
Revised: February 14, 2022
Published: February 24, 2022

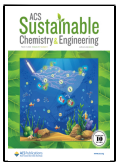

**Scheme 1. Suggested Overall Mechanism of a Catalytic Reaction between Furans with Alkenes over Acid Zeolites**[a]

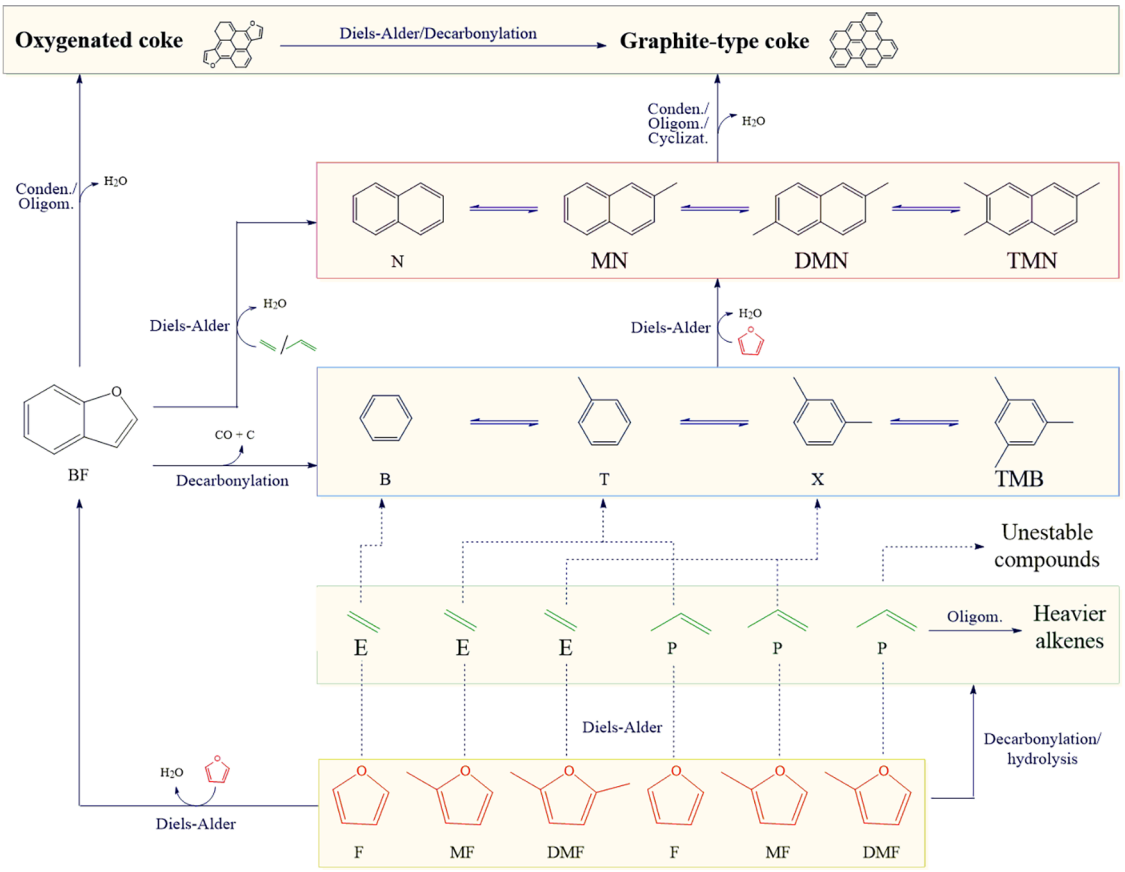


[a]Each family includes the structural isomers.

In this context, there is a good agreement about the positive influence of cofeeding high ratios of olefins, increasing the H/$C_{eff}$ ratio [$H/C_{eff} = (H - 2{\cdot}O)/C$].[24] Nevertheless, the mechanistic causes of this effect have not been elucidated yet. In parallel, the effect of furan alkylation has not been studied in the bibliography, although the same benefit on the catalytic stability could be expected since the H/$C_{eff}$ ratios of furan, methylfuran, and dimethylfuran are 0.5, 0.8, and 1.0, respectively. It should be noted that all of the furanic compounds studied in this work can be obtained from renewable resources.

In this paper, we perform a systematic study of the effect of the alkylation grade of both reactants on the furan and alkene aromatization. In addition to a deep analysis of the product distribution (to identify the relative weight of the different coke precursor routes), experimental results are focused on the stability and the deactivation mechanism. For performing a quick and quantitative comparison of the deactivation effects when working with different mixtures, we propose an empirical deactivation model able to consider the key issues of these reactions: very high reaction rates and fast deactivation. In the same way, the effects on the regeneration were studied, analyzing not only the calcination temperature but also the renewability of the catalyst in its activity and selectivity.

## MATERIALS AND METHODS

Commercial $NH_3$-ZSM-5 zeolite (Si/Al: 11.5, CBV2314, 0.19 $cm^3{\cdot}g^{-1}$, 353 $m^2{\cdot}g^{-1}$) was supplied by Zeolyst. The active form of the catalyst (H-ZSM-5) was obtained by air treatment at 550 °C for 12 h, the temperature being reached with a slope of 1 °C·$min^{-1}$. H-ZSM-5 powder was pelletized, crushed, and sieved in 250−355 $\mu$m aggregates. The catalyst (60 mg) was placed inside a 0.7 cm internal diameter of a U-shaped fixed-bed quartz reactor placed inside an electric oven equipped with a thermocouple and a PID controller. All of the pipes and fittings of the transfer line, reactor, and the analytic system were maintained at 250 °C with heating blankets to prevent any condensation and to produce flash vaporization of the reactants.

Furan (F), 2-methylfuran (MF), and 2,5-dimethylfuran (DMF) were purchased from Sigma-Aldrich with a purity higher than 99% in all of the cases. The furans were fed the line transfer using a syringe pump as mixed in a transfer line with ethylene (E) or propylene (P) as alkenes (Air Liquide, >99.5%).

In all experiments, the alkene/furan molar ratio was kept constant at 1:1. Helium (Air Liquide, >99.999%) was employed as a carrier gas, reaching a total flow of 20 N mL·$min^{-1}$ with an organic fraction of 10% (WHSV = 4.3−6.2 $h^{-1}$). The reaction temperature was held at 500 °C. The pressure was kept at 2.2 bar with a pressure drop lower than 0.2 bar along all of the systems.

Qualitative analyses were carried out by gas chromatography-mass spectrometry (GC-MS Shimadzu QP 2010) once the effluent was condensed with an ice bath and dissolved in organic solvents (acetone and octane for a complete identification). A capillary column was used as a stationary phase (TRB 5MS, 30 m, 0.25 mm). The quantitative analysis was carried out online by gas chromatography with a flame ionization detector (GC-FID HP 6890Plus), using the same column as in the GC-MS and commercial samples for calibration.

The different structural isomers of the different compounds are quantified together to simplify the analysis. The percentage of the known compound area was always higher than 96%, assuming that the discrepancies in the carbon balances were due to solid carbonaceous deposits, CO, $CO_2$, and/or condensed compounds (named coke and


https://doi.org/10.1021/acssuschemeng.1c08544
ACS Sustainable Chem. Eng. 2022, 10, 3057−3065

$CO_x$ for simplicity). Equations used to express the results are summarized below

$$\text{conversion: } x_a\ (\%) = \left(1 - \frac{C_{as}}{C_{a0}}\right) \times 100 \quad (1)$$

$$\text{carbon balance: CB } (\%) = \frac{\sum (n_i \cdot C_i) + n_{a1} \cdot C_{as1} + n_{a2} \cdot C_{a02}}{n_{a1} \cdot C_{a01} + n_{a2} \cdot C_{a02}} \times 100 \quad (2)$$

$$\text{selectivity: } \varphi_i(\%) = \frac{n_i \cdot C_i}{\sum (n_i \cdot C_i)} \times \text{CB} \times 100 \quad (3)$$

$$\text{benzenes alkylation grade: } \eta_{\text{Benz.}} = 0 \cdot \varphi_B + 1 \cdot \varphi_T + 2 \cdot \varphi_X + 3 \cdot \varphi_{TMB} \quad (4)$$

$$\text{naphth. alkylation grade: } \eta_{\text{Naph.}} = 0 \cdot \varphi_N + 1 \cdot \varphi_{MN} + 2 \cdot \varphi_{DMN} + 3 \cdot \varphi_{TMN} \quad (5)$$

In these equations, "C" is the concentration of the "i" compound in the gas phase or "a" reactant and "$n$" is the number of carbon atoms in the molecule. Therefore, selectivity is expressed in terms of moles of carbon. For comparison, it has been considered the reactant alkylation grade of the F-E reaction as "0"; "1" for MF-E and F-P; "2" for MF-P and DMF-E; and "3" for DMF-P.

Coke deposition was analyzed by temperature-programmed oxidation (TPO) analysis in a Micromeritics Autochem II 2920, using 30 mg of the spent catalyst in each analysis. A flow of 5% $O_2$ in helium (20 N mL·min$^{-1}$) was used as a reactive carrier gas, increasing the temperature up to 950 °C with a 5 °C·min$^{-1}$ slope. The $CO_2$ signal was followed by mass spectrometry (Omnistar GSD 301).

## RESULTS AND DISCUSSION

**Effect of the Reactant Alkylation Grade on the Activity and Selectivity.** Despite the pair furan−alkene used, an initial stable phase is observed (1.5−3 h, depending on the pair of reactants, as discussed below), reaching the total conversion of all of the furan compounds and stable values from 60 to 80% for the alkene.

The global selectivity in the stable period is shown in Figure 1. Parallel evolution is observed, benzenes being the main products in all of the cases, with an increased selectivity as the alkylation grades rise. Thus, the selectivity of benzenes for the MF-P system is 22% higher than that corresponding to MF-E (56.1 and 46%, respectively). This analysis is extrapolated to all of the pairs, comparing different alkylation grades of furans and alkenes. As a result, the selectivity obtained for the F-E mixture (43.4%) increases up to 55.2% for DMF-E and from 51.3% for F-P to 62.2% for DMF-P. This monoaromatic selectivity increase is directly related to the decrease in the coke and $CO_x$ fraction, and the changes in the selectivities for alkenes, naphthalenes, and indenes are less marked.

According to these data, there are no differences between considering the alkylation grade on furan or alkene, a conclusion demonstrated in the analysis of selectivity toward benzenes as a function of the alkylation grade (Figure 1b). In general terms, the selectivity to monocyclic aromatics increases as the alkylation of any reactant increases. This trend is also corroborated in the carbon balance closure, obtaining a clear declining trend of the relevance of coke and COx fraction as the alkylation grade increases, being independent of the alkylated reactant.

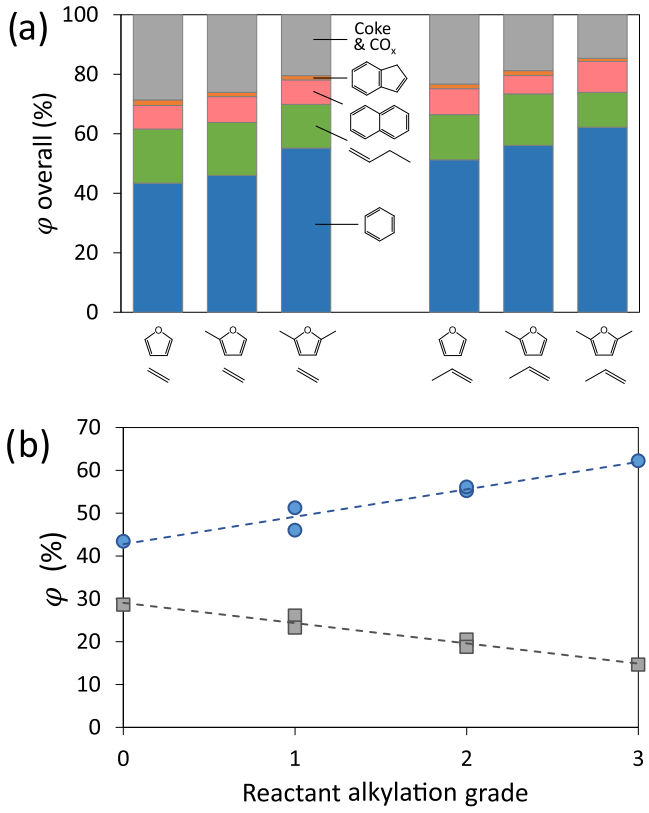


**Figure 1.** (a) Overall selectivity during the stable phase of furan and alkene reactions. Each family includes its alkylated derivates. (b) Selectivity to benzenes (solid blue circles) and coke and $CO_x$ (solid gray squares) depending on the reactant alkylation grade. Reaction conditions: 60 mg of H-ZSM-5, 500 °C, 2.2 atm, total flow 20 N mL·min-1, 10% reactants, alkene/furan molar ratio = 1:1.

Regarding the influence of the reactants on the product alkylation grade, Figure 2 illustrates the distribution of benzenes and naphthalenes (values detailed in the Supporting Information, Table S1), observing the anticipated increase in the substitution level of both families. Thus, the selectivity of benzene decreases from 27% (F-E) to 20% (DMF-E) and from 20% (F-P) to 17% (MF-P). The opposite trend is reached with high-alkylated benzene, trimethylbenzene (TMB), with a soft increase from 4 to 8% (from F-E to DMF-E) and from 4 to 6% when working with propylene. A parallel analysis can be done concerning the naphthalene family: naphthalene decreases from 37% (F-E) to 23% (MF-P), whereas dimethylnaphthalene increases from 16 to 32%, respectively.

In both cases, the DMF-P reaction is an exception, not following the general trend. The unstable character of the direct Diels−Alder intermediate (according to the reaction mechanism, this compound would have five substitutes in the carbon of the C−C bond) is considered to be the cause of this exception. This compound suffers dealkylation, producing the most stable intermediates, i.e., benzene and toluene (16 and 28.2%, respectively). This instability affects in the same way as benzenes and naphthalenes, in such a way that there is a direct influence on the benzene alkylation grade and the corresponding naphthalene ones. This fact is observed in Figure 2b, having a key impact on the reaction stability, as explained in the next section.

To sum up the previous discussion, the reactant and product alkylation grades are compared in Figure 3, considering the



https://doi.org/10.1021/acssuschemeng.1c08544
ACS Sustainable Chem. Eng. 2022, 10, 3057−3065

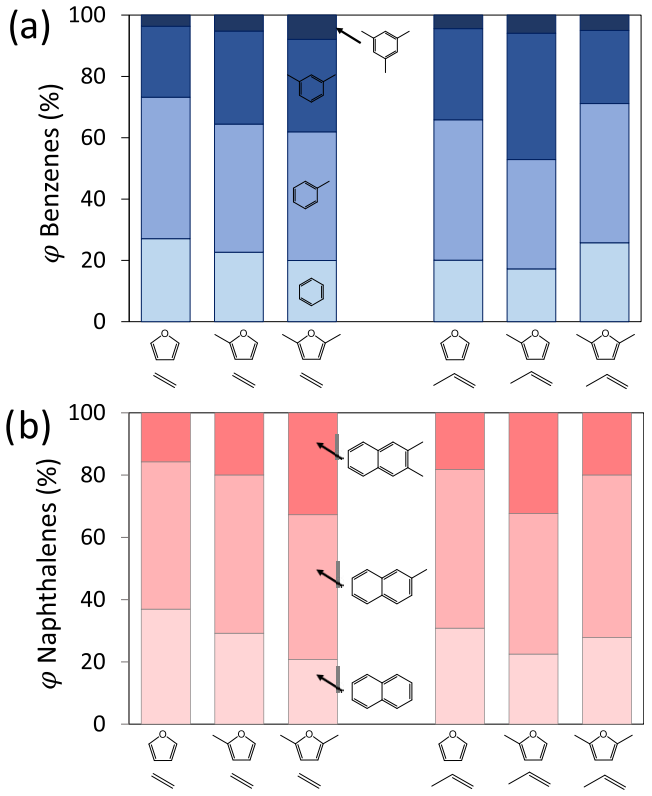


**Figure 2.** (a) Benzene and (b) naphthalene selectivity distribution during the stable phase of diverse reactions between furans and alkenes. Reaction conditions are summarized in Figure 1.

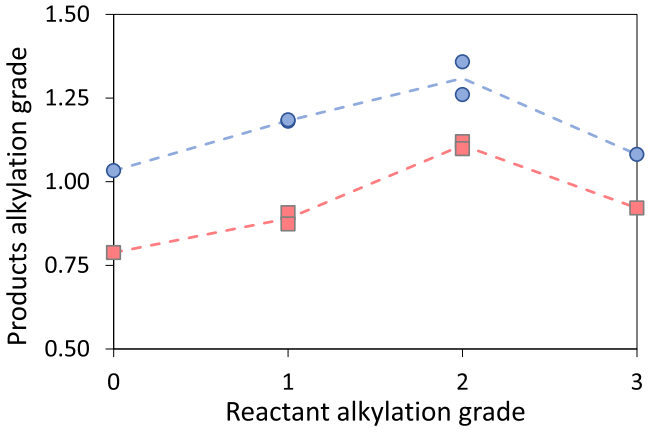


**Figure 3.** Benzene (solid blue circles) and naphthalene (solid pink squares) alkylation grade depending on the reactant alkylation grade for different furan−alkene reactions. Reaction conditions are summarized in Figure 1.

relative weight of each isomer in the total family of compounds, according to eqs 4 and 5. There is an increasing trend between both parameters, with the previously mentioned exception of DMF-P (alkylation grade of 3).

However, there is no clear correlation between the alkylation grade of reactants and the corresponding one of the products, in such a way that reactant alkylation grades of 2 produce average alkylation grades on the products lower than this value. This fact suggests an important influence of the alkylation/dealkylation reactions. For example, the direct reaction of a nonalkylated mixture (F-E) should result in products' 0 alkylation grade (benzene). However, it has been observed as a product alkylation grade of 1.03, indicating that the benzenes underwent some alkylation. On the contrary, MF-P and DMF-E reactions (reactant alkylation of 2) should result in xylenes (alkylation grade: 2). Nevertheless, the observed results were 1.36 and 1.26, respectively, indicating that the xylenes underwent dealkylation reactions.

The coexistence of more than one aromatic isomers in the reaction medium can explain the lack of correspondence between alkylation grades of reactants and products since the results can be affected by transalkylation mechanisms. However, alkenes are alkylation agents[25] and the relative weight of both phenomena cannot be isolated since both are catalyzed by the same acid sites of the zeolitic structure.

Despite the mechanism, the ZSM-5 effective pore size explains the prevalence of a higher alkyl grade in the family of benzenes than in naphthalenes. ZSM-5 zeolite has an average pore diameter of 5.4 Å (6.1 Å after applying the Norman radii correction that considers the swelling effect of the temperature on the structure), whereas BTX compounds have kinetic diameters from 5.9 to 7.1 Å (B, 5.9 Å; T, 5.9 Å; X, ∼6.4 Å; and TMB, ∼7.1 Å), slightly smaller than the naphthalene ones from 6.2 to 7.7 Å (N, 6.2 Å; MN, 6.8 Å; and DMN, 7.7 Å). Thus, shape selectivity constraints justify the lower alkylation grade observed with napthalenes, as well as the dealkylation trend of trimethylbenzenes into toluene and benzene. On the other hand, naphthalenes can be formed from benzene by a sequence of alkylation that finally cycle and form a second aromatic ring. In this way, a high-alkylated benzene results in low alkylated naphthalene.

**Effect of the Reactant Alkylation Grade on the Catalyst Deactivation.** During the first 1−2 h of reaction, the reactor operates at steady state, with a flat temporal profile of all of the reaction products. The temporal evolution of the aspect of the catalytic bed (Figure S1) is congruent with the formation of solid carbonaceous deposits as the main deactivation cause. In the first 2 h on stream, the catalyst shows a light gray color. As the reaction proceeds, the color of the catalyst becomes closer to the black color. At the end of the experiment (4 h), the catalyst is uniformly black, and the alkene conversion is negligible, whereas a residual furan conversion is observed (close 10%). At this point, no condensed compounds are detected in the gas phase and the disappearance of furan is assumed to be due only to the interaction of this compound with the coke previously deposited on the catalytic surface, increasing the coke accumulation. The evolution of reactant conversions with the time-on-stream (TOS) is shown in Figure 4.

The evolution of the conversion of both reactants vs time-on-stream was fit to an empirical model to numerically compare the stability trends in the different studied cases. For accomplishing this purpose, it was first considered that the loss of activity of a given catalyst was inversely correlated with the coke loading of the catalyst.[26] It should be noted that a kinetic deactivation model cannot be solved because of the complexity of the reaction mechanism. Thus, we have used the ratio between instantaneous and initial conversion (considering the residual activity when not negligible) instead of the activity.

$$\frac{(x - x_\infty)}{(x_0 - x_\infty)} = \frac{1}{1 + k \cdot C_{coke}} \quad (6)$$

In this equation, "$x$" is the conversion at any TOS, "$x_0$" is the initial value, and "$x_\infty$" is the stable conversion once the catalyst


https://doi.org/10.1021/acssuschemeng.1c08544
ACS Sustainable Chem. Eng. 2022, 10, 3057−3065

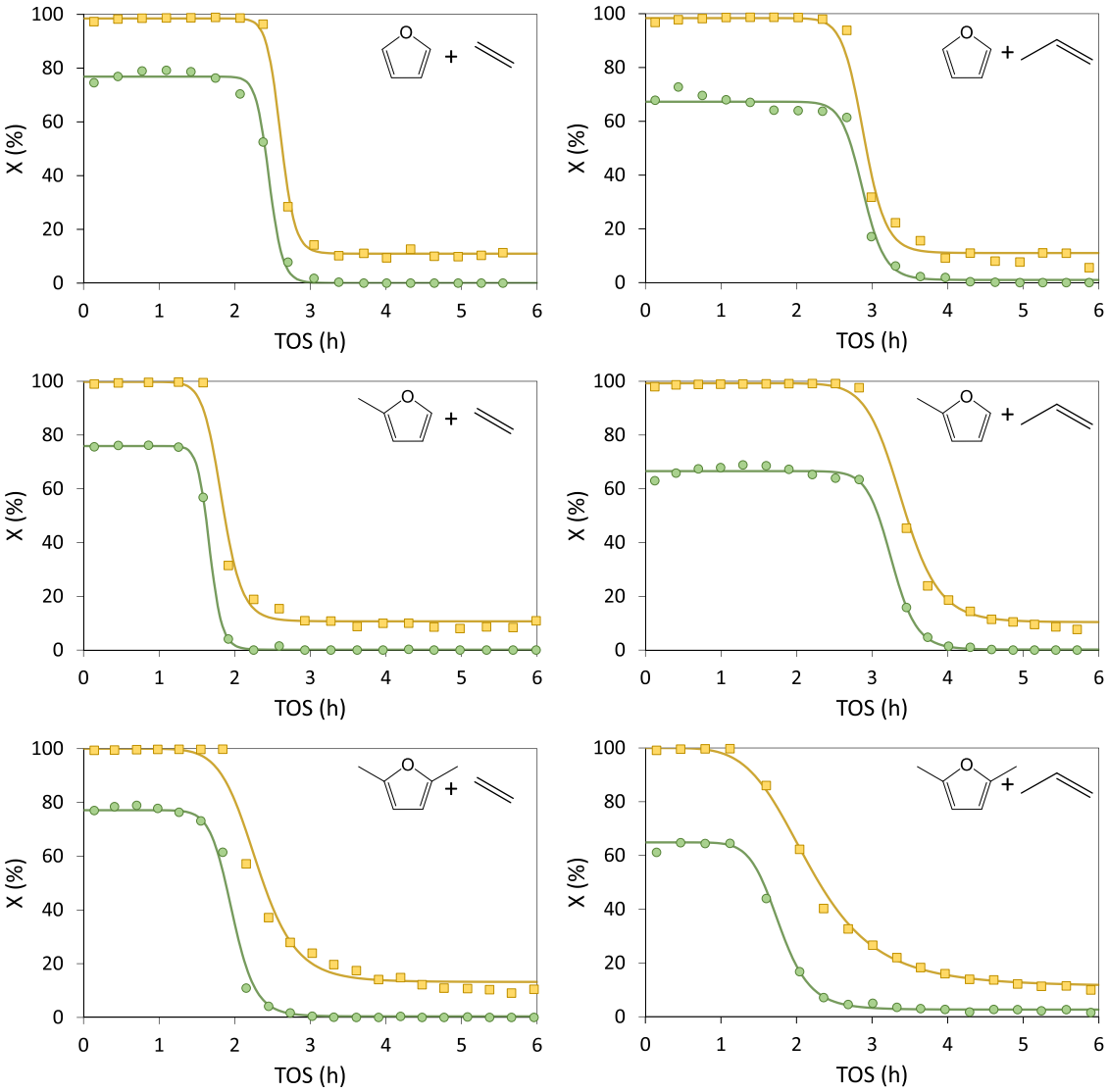


**Figure 4.** Evolution of furan (solid orange squares) and alkene (solid green circles) conversions with the TOS. Reaction conditions are summarized in Figure 1. Lines show proposed empirical model predictions.

is totally deactivated. These experimental values are reported in Table 1 for the different performed experiments.

**Table 1. Parameters of the Proposed Log-Logistic Model Adjusted to the Furans' Conversion for Different Furan–Alkene Reactions**

| | F-E | MF-E | DMF-E | F-P | MF-P | DMF-P |
|---|---|---|---|---|---|---|
| $x_0$ (%) | 98.5 | 99.8 | 100.0 | 98.4 | 99.3 | 100.0 |
| $x_{rem}$ (%) | 11.0 | 10.7 | 13.2 | 11.0 | 10.4 | 11.3 |
| $t_0$ (h) | 2.6 | 1.8 | 2.3 | 2.9 | 3.4 | 2.2 |
| $d$ | 28 | 14 | 9 | 20 | 14 | 5 |
| $\sigma$ (h) | 0.17 | 0.24 | 0.49 | 0.26 | 0.45 | 0.93 |
| $r^2$ | 0.998 | 0.993 | 0.990 | 0.995 | 0.999 | 0.998 |

On the other hand, coke production is conditioned by different reaction parameters, such as the temperature ($T$), the weight-space hourly velocity (WHSV), the time-on-stream (TOS), and the partial pressure of the coke precursor ($P$), furan in this case. Shao et al. proposed an exponential dependence, as detailed in eq 7.[27] In the case study, all of these parameters are constant, defining a new constant grouping all of these effects (eq 8).

$$C_{coke} = k \cdot e^{(a/T)} \cdot \mathrm{WHSV}^{b} \cdot P^{c} \cdot \mathrm{TOS}^{d} \tag{7}$$

$$C_{coke} = k' \cdot \mathrm{TOS}^{d} \tag{8}$$

Taking into account these premises, a log-logistic type deactivation model is proposed. The mathematical fit of this model with the experimental data demonstrates that the global constant corresponds to the inverse value of the distribution median time ($t_0$), a key point of the distribution corresponding to the time of the maximum depletion in conversion. Thus, the deactivation observed matches with eq 9

$$x = x_\infty + (x_0 - x_\infty) \cdot \frac{1}{1 + (\mathrm{TOS}/t_0)^{d}} \tag{9}$$

where $t_0$ and $d$ are the scale and shape parameters of the log-logistic distribution, respectively.[28] $t_0$ indicates the TOS in which it takes 50% of the deactivation, being an indicator of the period of stable activity of the catalyst. On the other hand, $d$ is an empirical power-law coefficient that defines the



https://doi.org/10.1021/acssuschemeng.1c08544
ACS Sustainable Chem. Eng. 2022, 10, 3057−3065

amplitude of the distribution. Nevertheless, the amplitude of the deactivation phase can be more specifically analyzed as a function of the typical deviation ($\sigma$) of the log-logistic distribution, according to eq 10. According to this expression, the deactivation rate decreases as the $\sigma$ increases.

$$\sigma = t_0 \cdot \left( \frac{(2\cdot\pi/d)}{\sin(2\cdot\pi/d)} - \frac{(\pi/d)^2}{\sin^2(\pi/d)} \right)^{1/2} \quad (10)$$

The values of these parameters for all of the reactions are included in Table 1 (furans) and the Supporting Information (alkenes, Table S2), as well as the regression coefficient of each fit. As expected, considering the shape of the curves and the assumptions of the empirical model, very close values of the parameters related to the deactivation rate were obtained for both reactants. By contrast, the differences are higher for the initial and final conversion.

The quality of the fit is observed in Figure 4, where the expected values according to the model adjustment are plotted as continuous lines.

The reported data suggest that the alkylation of both furan and olefin leads to improved catalyst stability. As discussed above, the increase of the product alkylation grade involves an increase in the benzene alkylation grade. In addition, as observed in Figure 5a, high-alkylated benzenes hinder naphthalene production. The reaction with the highest benzene alkylation grade (MF-P, 1.36) presented the lowest selectivity to naphthalenes (6.2%). On the contrary, DMF-P, with a benzene alkylation grade of 1.08 has a naphthalene selectivity of 10.4%. This trend is observed in all reactions, except the F-E reaction. This is expected to be due to the direct Diels–Alder reaction between furan and ethylene resulting in benzene, a very stable compound that does not further condensate to form naphthalenes.

Figure 5b demonstrates the relevance of naphthalenes on the catalytic stability as the higher naphthalene selectivity, the lower $t_0$, and the lower period of constant activity. Two different trends are distinguished, the stability being more sensitive to the naphthalene selectivity when using ethylene as an alkene but reaching higher $t_0$ when using propylene. It is concluded that propylene increases the stability of the system compared to ethylene, despite the furan used, reaching higher $t_0$ for the same selectivity of naphthalenes. Therefore, the most stable reactant combination is methylfuran with propylene.

This analysis is not so clear in terms of the reactant alkylation trend (Figure 5c). For intermediate situations, increasing the alkylation grade has a positive effect on the reaction stability ($t_{0,\text{MF-P}} > t_{0,\text{F-P}}$, $t_{0,\text{DMF-E}} > t_{0,\text{MF-E}}$). As occurred in the selectivity trends, F-E and DMF-P systems do not follow the general trend, observing a selectivity higher and lower than expected, respectively. The product distribution obtained with these pairs is suggested as the main cause of the observed discrepancies.

The previous analysis was focused on the time at which the conversion decreases to 50% of the original one ($t_o$). However, the influence of the reactants is extended to the deactivation rate, in such a way that the higher the alkylation grade, the softer the deactivation curve. A comparison of the zone of continuous deactivation for all of the performed experiments is shown in Figure 6a, observing that the deactivation rate also decreases as the alkylation grade increases, whereas it does not depend on the alkylated reactant (very similar curves obtained with MF-E and F-P, DMF-E and MF-P). This analysis can be

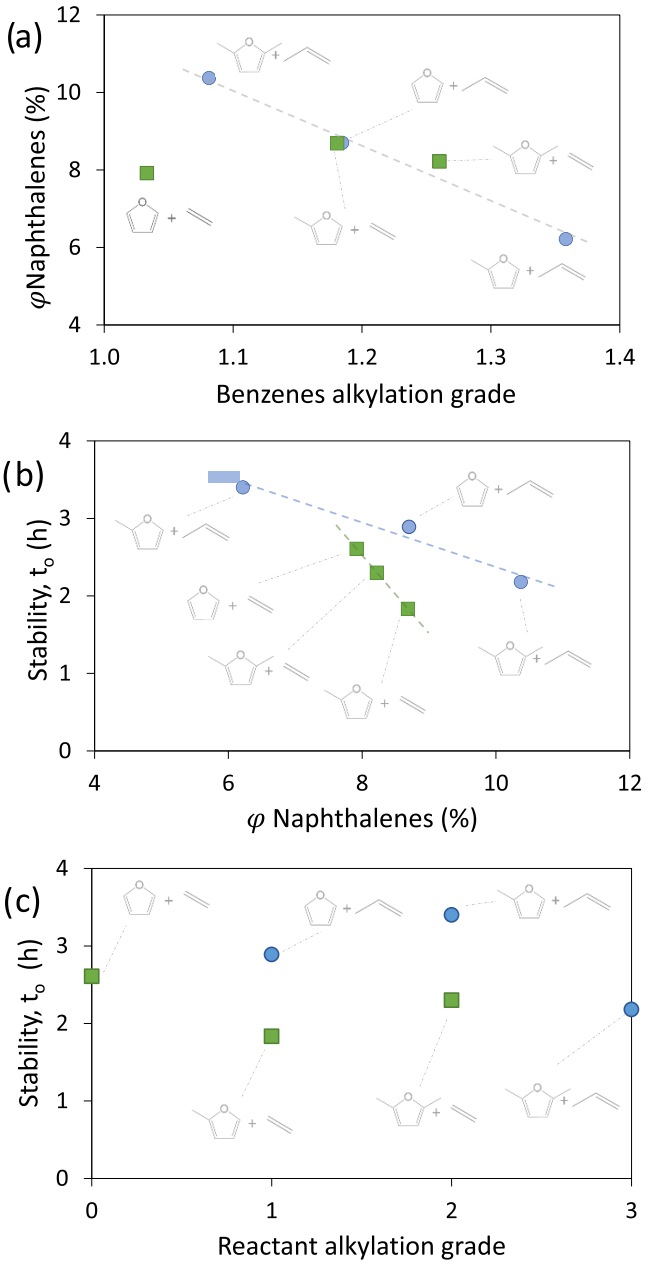


**Figure 5.** (a) Selectivity to naphthalenes as a function of the selectivity to benzenes. Analysis of reaction stability as a function of the (b) naphthalene selectivity and (c) reactant alkylation grade. Reaction conditions are summarized in Figure 1. Dashed lines are meant to serve as a visual reference.

corroborated in terms of deactivation phase duration ($\sigma$) observing a clear exponential increase with the reactant alkylation grade (Figure 6b). All of the $\sigma$ values are included in Table 1 from 0.17 h (F-E) to 0.93 h (DMF-P).

The deactivated catalysts (TOS = 6 h) were analyzed by temperature-programmed oxidation (TPO), obtaining $CO_2$ signals that indicate three different carbonaceous contributions, with oxidation temperatures at 430–500, 500–580, and 580–640 °C. All of the profiles are included in the Supporting Information (Figure S2) as well as the detailed deconvolution of each signal (Table S3).

The coke concentration of the catalysts increases as the alkylation grade decreases, which is in good agreement with the stability improvement observed for the most substituted



https://doi.org/10.1021/acssuschemeng.1c08544
ACS Sustainable Chem. Eng. 2022, 10, 3057–3065

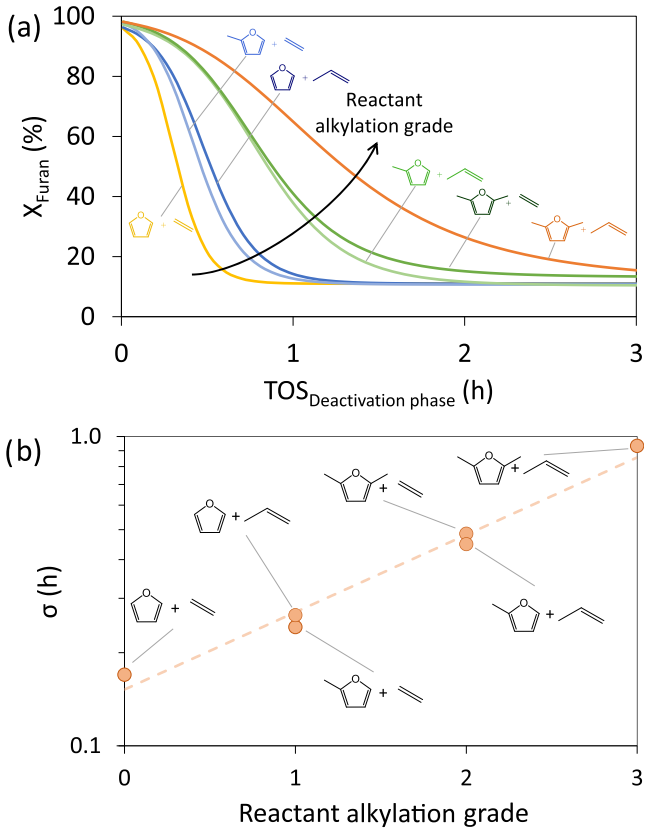


**Figure 6.** (a) Summary of furanic compound conversion evolution with TOS during the deactivation phase; (b) typical deviation of furan conversion adjusted to the log-logistic type model with the reactant alkylation grade (logarithmic scale). Reaction conditions are summarized in Figure 1. The dashed line is meant to serve as a visual reference.

reactants. In all of the cases, reactions involving propylene show a lower amount of coke produced than the corresponding ones using ethylene: 10.0, 7.0, and 3.3 mmol $CO_2$/g for F-E, MF-E, and DMF-E, respectively, and 8.2, 2.7, and 2.0 mmol $CO_2$/g for F-P, MF-P, and DMF-P, respectively. As for the type of coke, the decrease in the coke produced is always associated with an increment in the strength and stability of these carbonaceous deposits, as observed in Figure 7, with average combustion temperatures of 535, 560, and 570 °C for F-P, MF-P, and DMF-P, respectively.

As for the particular coke distribution and identification, two different types are observed. On the one hand, the highest combustion peak (610 °C) is 2 times higher when ethylene is used as alkene (2.5 ± 0.4 mmol $CO_2 \cdot g^{-1}$ vs 1.1 ± 0.1 mmol $CO_2 \cdot g^{-1}$). This peak has almost the same intensity despite the furan used, suggesting a correspondence with graphitic coke produced by alkene oligomerization (independent reaction with no influence of furan). This hypothesis agrees with previous works of Cheng and Huber,[7] where the strongest coke is identified as a graphitic-like one.

On the other hand, low combustion temperature deposits (535 and 560 °C) decrease as furan alkylation increases, both in reactions with ethylene and propylene. This fact indicates that these two peaks are highly conditioned by the furan (oxygenated coke). The lowest compaction and density of this type of coke justify its lower oxidation temperature.

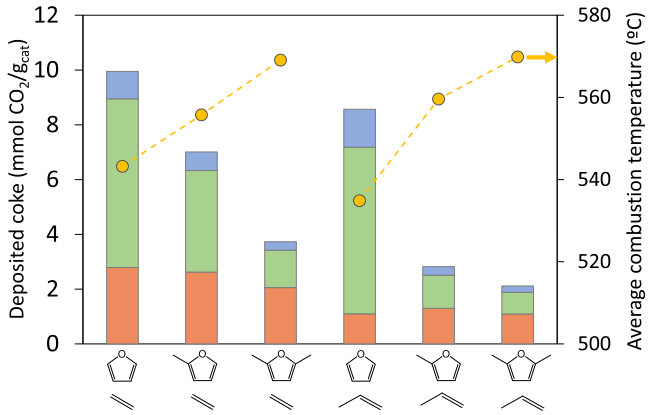


**Figure 7.** Deposited coke over the catalyst and average combustion temperature for diverse furan−alkene reactions. Combustion temperatures: 430−500 °C (blue), 500−580 °C (green), and 580−640 °C (orange). Reaction conditions are summarized in Figure 1.

**Evaluation of Catalyst Regenerability.** Finally, to evaluate the catalyst renewability, five reaction−regeneration cycles with the system methylfuran/propylene were considered. According to the TPO results, the regeneration was carried out at 650 °C for 20 min (ramp rate 5 °C/min from the reaction temperature) in air. This temperature ensures the combustion of the carbonaceous deposits in all of the mixtures tested in this work.

No significant permanent deactivation is observed, obtaining similar product distributions in the stable phase and quite analogous deactivation profiles for all of the cycles, as observed in Figure 8a. Thus, methylfuran is fully converted, whereas the stable phase corresponds to the conversion of propylene close to 65%, observing a progressive decrease in the last part of the cycle. This soft decrease is slightly more marked as the cycles advanced, without affecting neither the product distributions nor the deactivation time, but suggesting the presence of minor changes in the interaction of the coke precursors with the active sites upon regeneration procedures. Since the product distribution is not altered, this evolution is assumed as no relevant for the general reaction evolution. In all of the cycles, after the thermal regeneration, initial values are reached again. These results corroborate that the formation of carbonaceous deposits is the main deactivation cause, the acidity and zeolite structure not being significantly affected neither by its deposition nor by the thermal regeneration treatment. As for the selectivities, the results obtained at the end of the stable phase of each cycle are shown in Figure 8b. BTX is the major family observed in all of the cycles, with stable selectivities from 45 to 50%. The slight decreasing trend observed for naphthalenes (from 10 to 6%) matches with the slight increase in the coke and $CO_x$ fraction, suggesting a minimum increase in the coke produced by the oligomerization of this fraction. In any case, according to the conversion results, this partial blockage seems to be not relevant.

The $CO_2$ released during the regeneration has been monitored (Figure S3), observing maximum coke oxidation at 530−540 °C in all of the cycles, the organic deposits being almost completely removed when reaching the maximum temperature. The absence of thermal displacement discards the presence of stable deposits, expecting that this procedure could be implemented for a larger number of cycles without affecting the catalytic stability. These results are in good agreement with


https://doi.org/10.1021/acssuschemeng.1c08544
ACS Sustainable Chem. Eng. 2022, 10, 3057−3065

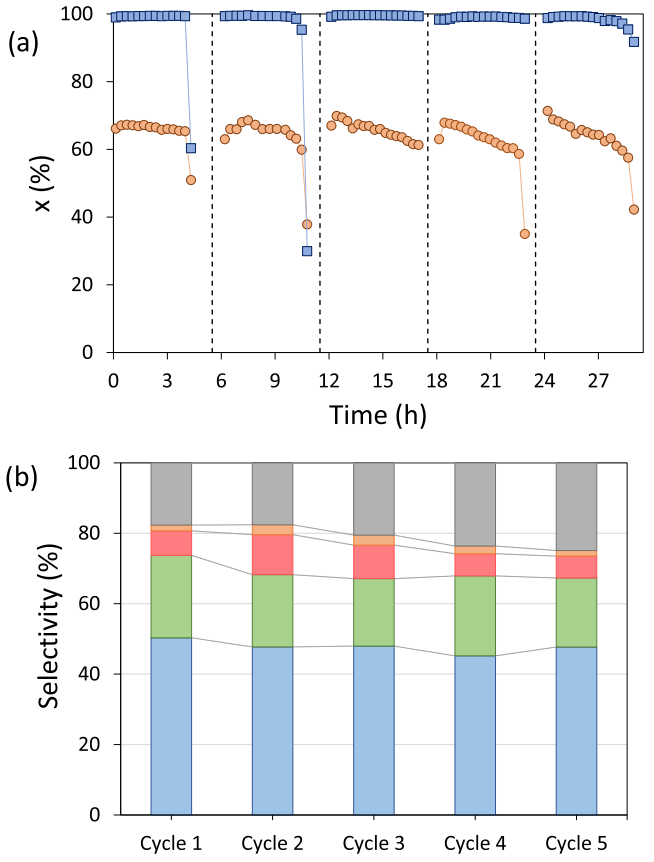


**Figure 8.** (a) Temporal evolution of methylfuran (blue) and propylene (orange) conversion. (b) Selectivity distribution obtained in the different cycles. Colors: Benzenes (blue), alkenes (green), naphthalenes (pink), indenes (orange), and coke and $CO_x$ gray). Reaction conditions are summarized in Figure 1.

the previous bibliography about furan or furans and methanol co-aromatization,[12,13] concluding that this approach involving heavier molecules improves the TOS in each cycle (for a similar furan WHSV, previous studies indicate deactivation periods of 1 h,[12] whereas this approach allows working more than 4 h before deactivation) without producing more stable coke that could prevent the catalytic reusability.

These results are considered as a good starting point of future works for the scale-up of this process. Based on the activity and stability profiles, a fluidized bed is considered as the optimum configuration, a well-known configuration already proposed for other bio-based processes with similar evolutions.[29] The continuous flow between reaction and regeneration phases could also enhance to reactivate the catalyst, ensuring the totally stable profiles of both reactants.

## CONCLUSIONS

This study has analyzed the influence of alkylation grade in the catalytic activity, selectivity, and coking kinetics of furan and alkene reactions. In general terms, the alkylation grade in the reactants has a positive effect on the benzene selectivities, mainly the alkylate ones, and this fact inhibits the formation of naphthalenes and indenes, both of them identified as coke precursors. A comprehensive deactivation study allows concluding that the increase in the stability not only affects time with stable conversion and product distribution but also the deactivation rate. Thus, the stable phase is extended with the alkylation grade, whereas the deactivation rate decreases. These facts allow increasing the control on the reaction, proposing stable reactions and regeneration cycles, which corroborate that the coke produced can be easily removed by a thermal treatment without altering the zeolite structure and surface chemistry. In global terms, the methylfuran−propylene reaction is proposed as the best one, obtaining stable phases up to 4 times higher than that proposed in the literature for similar systems, increasing the BTX selectivity by more than 50% with respect to the furan and ethylene co-aromatization.

## ASSOCIATED CONTENT

### Supporting Information

The Supporting Information is available free of charge at https://pubs.acs.org/doi/10.1021/acssuschemeng.1c08544.

Graphical evolution of the reaction over the catalyst bed; selectivities in the stable phase; log-logistic adjustment parameters; TPO's evolution and deconvolution of the spent catalyst; and TPOs of the regeneration cycles (PDF)

## AUTHOR INFORMATION

### Corresponding Author

**Salvador Ordóñez** − *Catalysis, Reactors & Control Research Group (CRC), Department of Chemical and Environmental Engineering, University of Oviedo, Oviedo 33006, Spain;* orcid.org/0000-0002-6529-7066; Phone: +34 985 103 437; Email: sordonez@uniovi.es

### Authors

**Juan Gancedo** − *Catalysis, Reactors & Control Research Group (CRC), Department of Chemical and Environmental Engineering, University of Oviedo, Oviedo 33006, Spain*

**Laura Faba** − *Catalysis, Reactors & Control Research Group (CRC), Department of Chemical and Environmental Engineering, University of Oviedo, Oviedo 33006, Spain*

Complete contact information is available at: https://pubs.acs.org/10.1021/acssuschemeng.1c08544

### Notes

The authors declare no competing financial interest.

## ACKNOWLEDGMENTS

This study was financially supported by the Spanish Ministry of Economy and Competitiveness (CTQ2017-89443-C3-2-R and MCI-21-PID2020-112587RB-I00). J.G. acknowledges the Spanish Ministry of Science and Innovation for the Ph.D. fellowship (PRE2018-084447).

## REFERENCES

(1) Settle, A. E.; Berstis, L.; Rorrer, N. A.; Roman-Leshkóv, Y.; Beckham, G. T.; Richards, R. M.; Vardon, D. R. Heterogeneous Diels−Alder catalysis for biomass-derived aromatic compounds. *Green Chem.* **2017**, *19*, 3468−3492.

(2) Román-Leshkov, Y.; Barrett, C. J.; Liu, Z. Y.; Dumesic, J. A. Production of dimethylfuran for liquid fuels from biomass-derived carbohydrates. *Nature* **2007**, *447*, 982−986.

(3) Mahmoud, E.; Yu, J. Y.; Gorte, R. J.; Logo, R. F. Diels-Alder and dehydration reactions of biomass-derived furan and acrylic acid for the synthesis of benzoic acid. *ACS Catal.* **2015**, *5*, 6946−6955.

(4) Huber, G. W.; Iborra, S.; Corma, A. Synthesis of transportantion fuels from biomass: chemistry, catalysts, and engineering. *Chem. Rev.* **2006**, *106*, 4044−4098.

(5) Gandarias, I.; García-Fernández, S.; Obregón, I.; Agirrezabal-Telleria, I.; Arias, P. L. Production of 2-methylfuran from biomass through an integrated biorefinery approach. *Fuel Process. Technol.* **2018**, *178*, 336−343.
(6) Rezaei, P. S.; Shafaghat, H.; Daud, W. M. A. W. Production of green aromatics and olefins by catalytic cracking of oxygenate compounds derived from biomass pyrolysis: A review. *Appl. Catal., A* **2014**, *469*, 490−511.
(7) Cheng, Y.-T.; Huber, G. W. Production of targeted aromatics by using Diels−Alder classes of reactions with furans and olefins over ZSM-5. *Green Chem.* **2012**, *14*, 3114−3125.
(8) Carlson, T. R.; Cheng, Y.-T.; Jae, J.; Huber, G. W. Production of green aromatics and olefins by catalytic fast pyrolysis of wood sawdust. *Energy Environ. Sci.* **2011**, *4*, 145−161.
(9) Shao, S.; Zhang, H.; Xiao, R.; Shen, D.; Zheng, J. Comparison of catalytic characteristics of biomass derivates with different structures over ZSM-5. *BioEnergy Res.* **2013**, *6*, 1173−1182.
(10) Foster, A. J.; Jae, J.; Cheng, Y.-T.; Huber, G. W.; Lobo, R. F. Optimizing the aromatic yield and distribution from catalytic fast pyrolysis of biomass over ZSM-5. *Appl. Catal., A* **2012**, *423*−*424*, 154−161.
(11) Kelkar, S.; Saffron, C. M.; Andreassi, K.; Li, Z.; Murkute, A.; Miller, D. J.; Pinnavaia, T. J.; Kriegel, R. M. A survey of catalysts for aromatics from fast pyrolysis of biomass. *Appl. Catal., B* **2015**, *174*−*175*, 85−95.
(12) Uslamin, E. A.; Luna-Murillo, B.; Kosinov, N.; Bruijnincx, P. C.; Pidko, E. A.; Weckhuysen, B. M.; Hensen, E. J. Gallium-promoted HZSM-5 zeolites as efficient catalysts for the aromatization of biomass-derived furans. *Chem. Eng. Sci.* **2019**, *198*, 305−316.
(13) Cheng, Y. T.; Jae, J.; Shi, J.; Fan, W.; Huber, G. W. Production of renewable aromatic compounds by catalytic fast pyrolysis of lignocellulosic biomass with bifunctional Ga/ZSM-5 catalysts. *Angew. Chem.* **2012**, *51*, 1387−1390.
(14) Li, J.; Yu, Y.; Li, X.; Wang, W.; Yu, G.; Deng, S.; Huang, J.; Wang, B.; Wang, Y. Maximizing carbon efficiency of petrochemical production from catalytic co-pyrolysis of biomass and plastics using gallium-containing MFI zeolites. *Appl. Catal., B* **2015**, *172*−*173*, 154−164.
(15) Espindola, J. S.; Gilbert, C. J.; Perez-Lopez, O. W.; Trierweiler, J. O.; Huber, G. W. Conversion of furan over gallium and zinc promoted ZSM-5: The effect of metal and acid sites. *Fuel Process. Technol.* **2020**, *201*, No. 106319.
(16) Zhang, B.; Zhong, Z.; Xie, Q.; Chen, P.; Ruan, R. Reducing coke formation in the catalytic fast pyrolysis of bio-derived furan with surface modified HZSM-5 catalysts. *RSC Adv.* **2015**, *5*, 56286−56292.
(17) Yu, J.; Zhu, S.; Dauenhauer, P. J.; Cho, H. J.; Fan, W.; Gorte, R. Adsorption and reaction properties of SnBEA, ZrBEA and H-BEA for the formation of p-xylene from DMF and ethylene. *Catal. Sci. Technol.* **2016**, *6*, 5729−5736.
(18) Green, S. K.; Patet, R. E.; Nikbin, N.; Williams, C. L.; Chang, C.-C.; Yu, J.; Gorte, R. J.; Caratzoulas, S.; Fan, W.; Vlachos, D. G.; et al. Diels−Alder cycloaddition of 2-methylfuran and ethylene for renewable toluene. *Appl. Catal., B* **2016**, *180*, 487−496.
(19) Xu, M.; Mukarakate, C.; Iisa, K.; Budhi, S.; Menart, M.; Davidson, M.; Robichaud, D. J.; Nimlos, M. R.; Trewyn, B. G.; Richards, R. M. Deactivation of multilayered MFI nanosheet zeolite during upgrading of biomass pyrolysis vapors. *ACS Sustainable Chem. Eng.* **2017**, *5*, 5477−5484.
(20) Du, S.; Gamliel, D. P.; Giotto, M. V.; Valla, J. A.; Bollas, G. M. Coke formation of model compounds relevant to pyrolysis bio-oil over ZSM-5. *Appl. Catal., A* **2016**, *513*, 67−81.
(21) Kasipandi, S.; Cho, J. M.; Park, K. S.; Shin, C. H.; Bae, J. W. Unprecedent activity and stability on zirconium phosphates grafted mesoporous silicas for renewable aromatics production from furans. *J. Catal.* **2020**, *385*, 10−20.
(22) Cheng, Y.-T.; Huber, G. W. Chemistry of furan conversion into aromatics and olefins over HZSM-5: a model biomass conversion reaction. *ACS Catal.* **2011**, *1*, 611−628.
(23) Gancedo, J.; Faba, L.; Ordóñez, S. Benzofuran as deactivation precursor molecule: Improving the stability of acid zeolites in biomass pyrolysis by co-feeding propylene. *Appl. Catal., A* **2021**, *611*, No. 117980.
(24) Zhang, H.; Cheng, Y.-T.; Vispute, T. P.; Xiao, R.; Huber, G. W. Catalytic conversion of biomass-derived feedstocks into olefins and aromatics with ZSM-5: the hydrogen to carbon effective ratio. *Energy Environ. Sci.* **2011**, *4*, 2297−2307.
(25) Degnan, T. F., Jr.; Smith, C. M.; Venkat, C. R. Alkylation of aromatics with ethylene and propylene: recent developments in commercial processes. *Appl. Catal., A* **2001**, *221*, 283−294.
(26) García-Dopico, M.; Garcia, A.; García, A. S. Modelling coke formation and deactivation in a FCCU. *Appl. Catal., A* **2006**, *303*, 245−250.
(27) Shao, S.; Zhang, H.; Wang, Y.; Xiao, R.; Heng, L.; Shen, D. Catalytic pyrolysis of biomass-derived compounds: coking kinetics and formation network. *Energy Fuels* **2015**, *29*, 1751−1757.
(28) Muse, A. H.; Mwalili, S. M.; Ngesa, O. On the log-logistic distribution and its generalizations: a survey. *Int. J. Stat. Probability* **2021**, *10*, 93.
(29) Caudle, B.; Gorensek, M. B.; Chen, C. C. A novel approach to modeling biomass pyrolysis in a fluidized bed reactor. *ACS Sustainable Chem. Eng.* **2020**, *8*, 14605.




https://doi.org/10.1021/acssuschemeng.1c08544
*ACS Sustainable Chem. Eng.* 2022, 10, 3057−3065